

## Interlayer exchange coupling mediated by valence-band electrons

J. Blinowski

*Institute of Theoretical Physics, Warsaw University, ul. Hoża 69,00-681 Warszawa, Poland*

P. Kacman

*Institute of Physics, Polish Academy of Sciences, al. Lotników 32/46, 02-668 Warszawa, Poland*

(Received 10 November 2000; published 13 June 2001)

The interlayer exchange coupling mediated by valence-band electrons in all-semiconductor IV-VI magnetic/nonmagnetic superlattices is studied theoretically. A three-dimensional tight-binding model, accounting for the band and magnetic structure of the constituent superlattice components is used to calculate the spin-dependent part of the total electronic energy. The antiferromagnetic coupling between ferromagnetic layers in EuS/PbS superlattices is obtained, in agreement with the experimental evidences. The results obtained for the coupling between antiferromagnetic layers in EuTe/PbTe superlattices are also presented.

DOI: 10.1103/PhysRevB.64.045302

PACS number(s): 68.65.-k, 75.70.-i, 75.25.+z

### I. INTRODUCTION

Interlayer exchange coupling (IEC) was discovered in late 1980's in Fe/Cr/Fe trilayers.<sup>1</sup> Since then, it has been observed in a variety of multilayer structures composed of alternating magnetic and nonmagnetic layers. These studies concentrated on the coupling between ferromagnetic, metallic layers, although separated by both metallic and insulating spacers. Thus, the ferromagnetic character of the magnetic layers and the fact that in these structures the Fermi level was situated in the region of high density of electronic states inhered to the theoretical models, which were designed to explain the origins of the IEC phenomena (see Ref. 2 and the references therein). Surprisingly enough, the IEC was also discovered in all-semiconductor superlattices (SL's). Moreover, the semiconductor SL's in which it was first observed were the MnTe/CdTe,<sup>3</sup> MnTe/ZnTe,<sup>4</sup> and EuTe/PbTe,<sup>5</sup> all with antiferromagnetic layers. Recently, such coupling was also identified in semiconductor multilayer structures with ferromagnetic EuS,<sup>6,7</sup> and Ga(Mn)As layers.<sup>8</sup> While the IEC in the trilayer Ga(Mn)As/Ga(Al)As/Ga(Mn)As with the high concentration of free carriers,<sup>8</sup> can be, at least qualitatively, explained in terms of the models tailored for metallic systems, the other semiconductor structures exhibiting IEC call for a different approach.

Several attempts to explain IEC in all-semiconductor structures have already been reported in the literature. Two models, in which the interlayer coupling is mediated by carriers localized on shallow impurities in the spacer region, were proposed for II-VI SL's.<sup>9,10</sup> These models do not apply to IV-VI structures, with the PbTe and PbS spacers, since in lead chalcogenides, localized shallow impurity states were never detected.<sup>11</sup> The calculations of the difference between total electronic energies obtained for two different (e.g., *B1* and *B2* in Fig. 1) spin configurations of the SL, performed within a frame of a very simple, one-dimensional (1D) tight-binding model, put first in evidence the significant role of the valence-band electrons in IEC in all-semiconductor magnetic/nonmagnetic layer structures.<sup>12</sup> This role was further demonstrated for EuTe/PbTe/EuTe trilayers by Wilczyński and Świrkowicz in Ref. 13, where a 3D tight-binding

model, still oversimplifying the band structure, was used. A different approach to the magnetic interlayer interactions mediated by valence electrons has been chosen by Dugaev *et al.*<sup>14</sup> These authors studied the Blombergen-Rowland mechanism within the effective-mass approximation and obtained a ferromagnetic coupling between two magnetic impurities situated at the opposite interfaces of a narrow-gap IV-VI semiconductor spacer. As the experimentally observed IEC in EuS/PbS SL's is antiferromagnetic,<sup>6,7</sup> this means that the Blombergen-Rowland interactions are not dominating IEC in these SL's. In this situation, the total energy calculations, which do not focus on a particular interaction mechanism but account globally for the spin-dependent structure of valence bands, seem to constitute the most appropriate approach. The calculations of this type, reported in Refs. 12 and 13, were clearly oversimplified and performed for a different spin structure than that of EuS/PbS (001) SL.

In this paper we present the results of refined 3D total-energy calculations, which take into account the crystal and the band structures of the SL's component materials. The tight-binding model with its assumptions and the results for three different spin structures, corresponding to all experi-

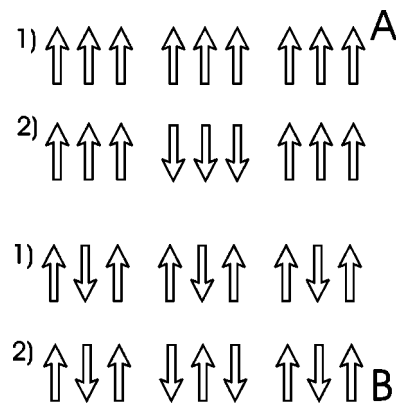


FIG. 1. The correlated colinear spin structures for (A) ferromagnetic and (B) antiferromagnetic layers. For the "in-phase" spin structures *A1* and *B1*, the magnetic period is equal to the chemical one, for the "out-of-phase" spin structures *A2* and *B2*, the magnetic period is two times larger.

mentally studied IV-VI semiconductor magnetic/nonmagnetic SL's, are presented in Sec. III. In Sec. II the magnetic and band structures of the constituent materials are described and the SL geometry is specified. The comparison with experimental data and the conclusions are presented in the last section.

## II. CONSTITUENT MATERIALS AND THE SUPERLATTICES GEOMETRY

All the components of the EuX/PbX SL's, where  $X = \text{Te}$  or  $\text{S}$ , crystallize in the rock-salt structure. Bulk PbS and PbTe are narrow gap nonmagnetic semiconductors with very similar band structures. They both have a direct energy gap between the  $p$ -anion valence band and the  $p$ -cation conduction band at the point  $L$  of the Brillouin zone (BZ).<sup>15,16</sup>

Bulk EuS is a classical Heisenberg ferromagnet with the Curie temperature 16.6 K.<sup>17</sup> Bulk EuTe exhibits Type-II antiferromagnetic (AFM) structure with the Néel temperature 9.6 K.<sup>17</sup> In EuTe, the spins of Eu ions are ferromagnetically ordered in (111)-type planes, which in turn are coupled antiferromagnetically to one another. All the Eu chalcogenides are semi-insulating, large-gap semiconductors. The results of the nonrelativistic augmented plane wave (APW) calculations of the EuS spin-polarized band structure<sup>18</sup> show the narrow  $f(\uparrow)$  bands situated in the energy gap between the valence band, formed essentially of anion  $p$  states, and the conduction band, built mostly of cation  $d$  states. The valence-band maximum is situated at the center of the Brillouin zone (BZ) and the conduction-band minimum at the point  $X$ . The spin splitting of the valence band results predominantly from the spin-dependent mixing of  $p$ -anion and  $f$ -cation states, whereas that of the conduction band is mostly due to  $f$ - $d$  and  $s$ - $d$  on-site direct exchange. Much less is known about the EuTe band structure. The optical experiments performed at  $T = 300$  K indicate,<sup>19</sup> that in the paramagnetic phase of EuTe, the  $f$ - $d$  gap is somewhat larger than in EuS, in agreement with the general trends visible in the experimental data<sup>17</sup> and the results of APW calculations for other europium chalcogenides.<sup>18</sup> These trends seem not to be followed in the recent<sup>20</sup> calculations of EuTe band structure, focused predominantly on the conduction bands.

Two types of EuS/PbS SL's were experimentally studied, one grown on KCl substrate along [001] and the other on BaF<sub>2</sub> along the [111] crystallographic axis. The measurements show that in both cases, the ferromagnetically ordered Eu spins within each magnetic layer lie in the planes perpendicular to the growth axis.<sup>21</sup> In the (001) structures, each atomic monolayer consists of both anions and cations, with the monolayers  $a/2$  apart, where  $a$  is the cubic lattice constant. The schematic view of two such monolayers is presented in Fig. 2. The distances between the cation and its four in-plane nearest neighbors (anions) and four in-plane next-nearest neighbors (cations) are also shown in the figure. The spin structure of the magnetic (001) SL, which corresponds to the observed antiferromagnetic interlayer coupling is shown schematically in Fig. 1, A2.

In the case of (111) EuS/PbS SL's IEC has not been yet observed. These SL's have the same crystallographic struc-

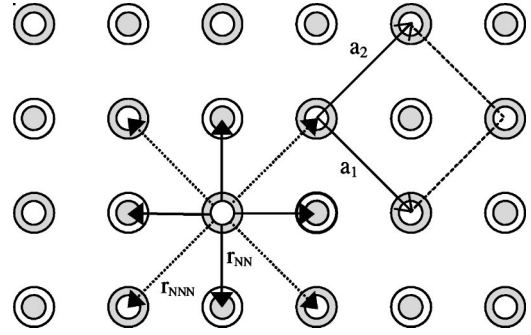


FIG. 2. Schematic view of two successive atomic layers of the EuS/PbS SL grown along [001] axis. The solid gray circles represent anions, the white circles cations—small circles are for ions in upper layer, the big ones for ions in the other. The distances  $r_{NN}$  from a cation to the four in-plane  $NN$  anions are shown by solid lines, by dotted lines the distances  $r_{NNN}$  to the in-plane  $NNN$  cations.  $\mathbf{a}_1$  and  $\mathbf{a}_2$  are the in-plane primitive lattice vectors.

ture as the experimentally studied EuTe/PbTe SL's grown along the [111] axis. With this growth direction, the subsequent (111) atomic monolayers are built either of anions or of cations, in alternation. The distance between cation and anion monolayers is  $a\sqrt{3}/6$ . A schematic view of three successive cation layers is presented in Fig. 3—the analogous anion sublattice is shifted by  $a\sqrt{3}/2$  along the [111] direction and is not shown in the figure for clarity reasons.

In EuTe/PbTe SL's the neutronographic measurements show that the AFM Type II structure is preserved in each EuTe layer and the ferromagnetic (FM) spin sheets form exclusively on the (111) planes parallel to the layers. For the nonmagnetic spacers thin enough, the neutronographic spectra clearly indicate the existence of some long-range order proving that the spins in consecutive magnetic layers are not randomly oriented, but tend to align along the same direction in a correlated way.<sup>5</sup> Although for the antiferromagnetic layers the notions of AFM and FM IEC are not applicable, two types of collinear correlated spin orientations in successive layers are still possible: identical (in-phase) and reversed (out-of-phase), as shown in Fig. 1, B1. Both types of IEC were observed in the experiment.

All the  $(\text{EuX})_m/(\text{PbX})_n$  SL's (where  $m$  and  $n$  denote the

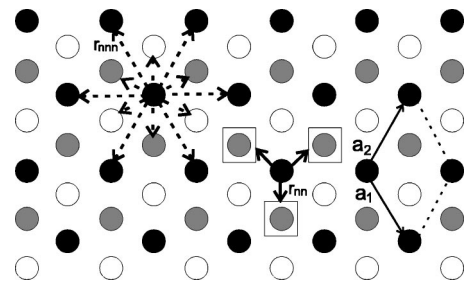


FIG. 3. Schematic view of the crystallographic structure of the EuX/PbX (111) SL's. The ions in three successive cation planes are represented by gray, black, and white circles, respectively. Only three  $NN$  anions, lying in the layer  $a\sqrt{3}/6$  above the black cation plane, are shown by open squares. The distances to all 12  $NNN$  are marked by dotted lines.

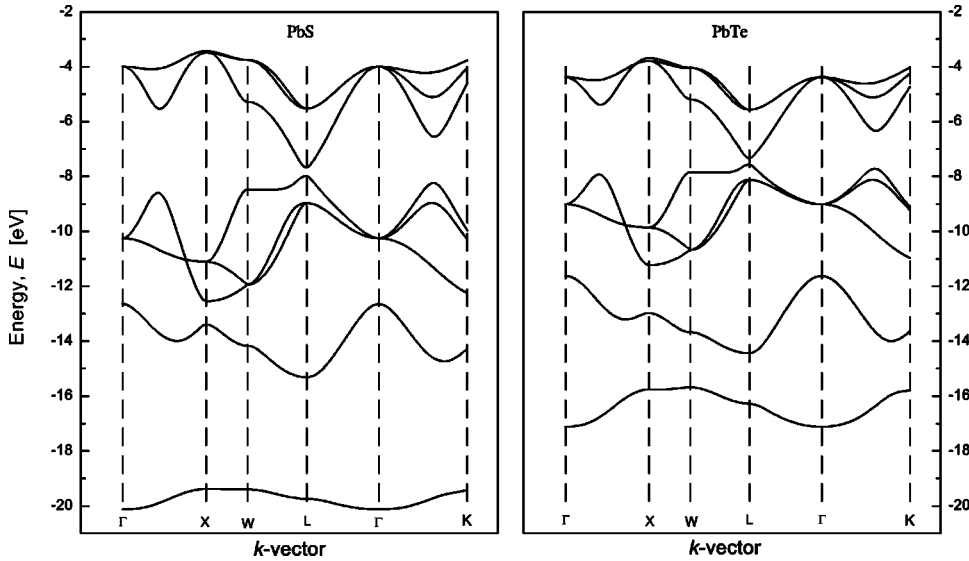


FIG. 4. Model band structures of PbS and PbTe.

number of EuX and PbX layers, respectively) have relatively small lattice mismatch. This mismatch, as well as the strains resulting from it, will be ignored in the following, though the strains were shown to affect the magnetic properties of the EuX layers, and their transition temperatures to the paramagnetic state.<sup>21,22</sup>

To discuss the spin coupling between the magnetic layers, one has to consider a SL magnetic elementary cell containing at least two such layers. In SL's grown along the [001] crystallographic direction, the situation is simple, as the stacking sequence is *ABAB* type. Such stacking does not enlarge the size of the magnetic elementary cell, whatever the  $m+n$  value. In contrast, the stacking sequence *ABCABC* type (compare Fig. 3) for both anions and cations, in SL's grown along the [111] axis does enlarge the elementary cell when  $m+n$  is not a multiple of 3. Thus, to limit the size of elementary cells, we consider only the (111) SL's with  $(n+m)/3 = \text{integer}$ . For both types of SL, our magnetic elementary cells contain  $2(m+n)$  anions,  $2m$  magnetic cations and  $2n$  nonmagnetic cations.

In order to determine IEC in the above structures we compare the total valence-electron energies in two magnetic SL's: with the in-phase and out-of-phase spin ordering. For the  $n$  and  $m$  values typical for the experimentally studied SL's, the elementary cells contain several tens of atoms. In view of this complexity, we decide to use the simplest calculation scheme still leading to a fairly realistic band structure, namely, an empirical tight-binding method. Even though the one-electron methods are not designed for the total-energy calculations, the small spin-dependent changes in the total energy should be described adequately within this approach.

### III. TIGHT-BINDING MODEL

To construct the empirical tight-binding Hamiltonian matrix, one has to select the set of atomic orbitals for every type of involved ions and to specify the range of the ion-ion interactions. This selection is always a compromise between the best description of the band structure and the minimiza-

tion of the Hamiltonian matrix dimensions and of the number of parameters used. In the following, we assume that the proper description of SL band structure is reached when the Hamiltonian reproduces in the  $n=0$  and  $m=0$  limits, the known band structures of the bulk constituent magnetic and nonmagnetic materials, respectively. This criterion determines, in principle, the selection of the ionic orbitals and gives the values of the parameters, all but those characterizing the interaction between magnetic and nonmagnetic cations.

To calculate the band structure of the lead chalcogenides (PbS and PbTe) we took into account  $s$  and  $p$  orbitals for both anions and cations, which lead to an  $8 \times 8$  Hamiltonian matrix. We allowed for the  $s-s$ ,  $s-p$ , and  $p-p$  anion-cation nearest-neighbor (NN) interactions and the anion-anion and cation-cation  $p-p$  next-nearest-neighbor (NNN) interactions. It turned out that the band structure can be reproduced much better when we include also, by second-order perturbation, the interactions of  $p$  orbitals with the three NN  $d$  orbitals belonging to the  $F_2$  representation. The values of the parameters describing all these interactions and the values of the on-site orbital energies were determined by an  $\chi^2$  minimization procedure, in which the band structure was fitted to the energies in the high symmetry points of the BZ, taken from Refs. 16 and 15. The obtained energy bands for PbS and PbTe along the symmetry axes of the BZ, are presented in Fig. 4.

In the other limit, for europium chalcogenides (EuS and EuTe), to describe the cations we take explicitly one  $s$  and five  $d$  orbitals, whereas the anions are described as before by  $s$  and  $p$  orbitals. The NN interaction involving the anion  $p$  orbitals and cation  $s$  and  $d$  orbitals as well as the NNN cation-cation  $d-d$  and anion-anion  $p-p$  interaction were included in the  $10 \times 10$  Hamiltonian. The  $s$ -anion- $s$ -cation,  $s$ -anion- $d$ -cation interactions, turned out to be less important and were neglected. Instead, we included, again by second-order perturbation, the hybridization of anion  $p(\uparrow)$  orbitals with the cation  $f(\uparrow)$  orbitals—this was necessary for reproducing the spin splittings of the valence bands in the ferro-

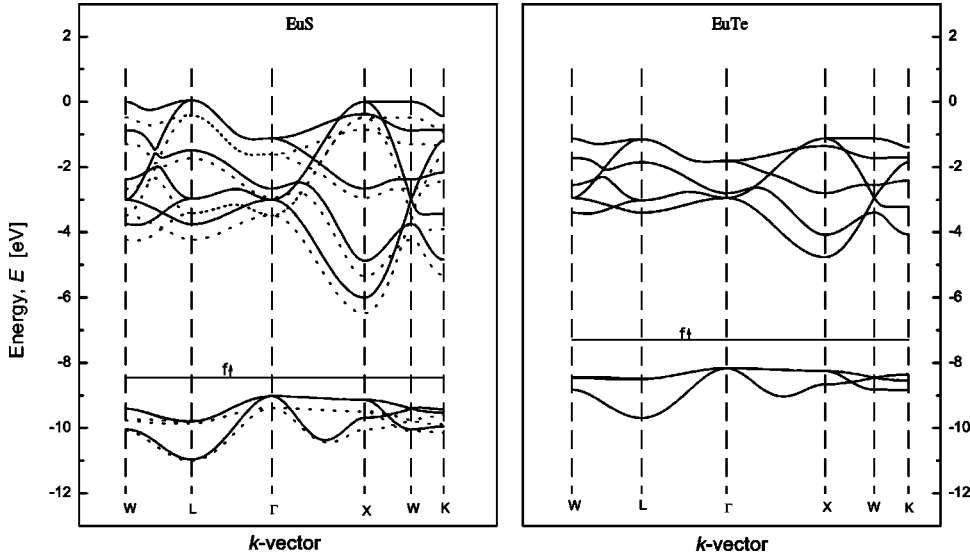


FIG. 5. Model band structures of ferromagnetic EuS (solid lines represent the spin-down bands; dotted lines—spin-up bands) and paramagnetic EuTe.

magnetic EuS [we neglected the hybridization with the energetically distant  $f(\downarrow)$  band]. To reproduce the spin splittings in the EuS conduction bands, the on-site exchange constants  $J_s$  and  $J_d$  had to be introduced. The band structure of EuS, presented in Fig. 5, was obtained with the parameters fitted to the results of the APW spin-polarized calculations reported in Ref. 18. The band structure of EuTe, presented in Fig. 5, was obtained with the parameter values extrapolated from the values for EuS and EuSe by exploiting the chemical trends in europium chalcogenides. The elementary cell of the antiferromagnetic EuTe has a twice larger volume and completely different shape than the one of the ferromagnetic EuS—to facilitate the comparison with EuS, we present the band structure of EuTe in the paramagnetic phase.

In the above, the number of independent fitting parameters was partially reduced according to the Harrison relations,<sup>23</sup> e.g., instead of two NNN interatomic matrix elements  $pp\sigma$  and  $pp\pi$ , we used  $pp\sigma = -4pp\pi$ . The constants describing the nonmagnetic cation-magnetic cation interactions were estimated from Harrison's formula for interatomic matrix elements. It has to be also noted, that in all calculations, we neglected the spin-orbit terms, known to be important in lead chalcogenides. These terms would increase the number of model parameters and double the matrix dimensions and would, therefore, pose a problem in the case of the SL's. Fortunately, we are mainly interested in valence bands, for which the spin-orbit is much less important than for the conduction bands. In the magnetic elementary cell of the  $(\text{EuX})_m/(\text{PbX})_n$  SL there are  $4(m+n)$  non-equivalent ions. In principle, seven orbitals ( $s, p, d$ ) should be taken into account for each anion and each nonmagnetic cation and 13 ( $s, d$ , and  $f$ ) for each magnetic cation. Using the second-order perturbation theory, we reduced the SL tight-binding Hamiltonian to the  $(20m+16n) \times (20m+16n)$  matrix. To determine the small difference between the large total energies of the valence electrons in the two, in-phase, and out-of-phase spin configurations, we did not calculate these energies separately. Instead, the difference between the two energies of the valence electrons was calculated at a given  $k$  point, after the numerical diagonalization

of the two corresponding Hamiltonian matrices and summation of the occupied states' energies. The results, obtained for a mesh of  $k$  points (16 000 points in the case of the tetragonal BZ of the  $(001)$   $(\text{EuS})_m/(\text{PbS})_n$  SL's, and 17 280 in the case of the hexagonal BZ of the  $(111)$   $(\text{EuS})_m/(\text{PbS})_n$  and  $(\text{EuTe})_m/(\text{PbTe})_n$  SL's), were then used in the triple Simpson procedure for integrating over the entire BZ.

We denote by  $\Delta E$  the absolute value of the energy difference between the in-phase and out-of-phase spin configuration per unit surface of the layer.  $\Delta E$  can be regarded as a measure of the strength of the interlayer spin coupling in the SL's—for ferromagnetic structures it can be expressed in terms of the constant  $J_1$ ,<sup>24</sup> commonly used to characterize the IEC in metallic magnetic/nonmagnetic trilayers by the relation:  $\Delta E = 4|J_1|$  (here, the factor 4, instead of 2, accounts for the fact that in SL each magnetic layer is coupled to two neighboring layers).

The sign of the calculated energy difference determines the spin configuration in consecutive magnetic layers. In the ferromagnetic EuS-based SL's, the out-of-phase spin configuration in consecutive magnetic layers is energetically preferred, so that IEC in these structures has an antiferromagnetic character, in agreement with the experiment. For the antiferromagnetic, EuTe-based SL's, the situation is more complicated: for odd number  $m$  of spin planes in the magnetic layer, the out-of-phase configuration has the lower energy, whereas for even  $m$  it is the in-phase configuration, which is energetically favored. Thus, one can notice that in all studied SL's the valence electron mediated IEC prefers the spin configuration with the opposite directions of spins at the two interfaces bordering the spacer.

Many various  $m$  and  $n$  values were selected to study the range of the interlayer coupling and the IEC dependence on the thickness of the magnetic layer. It turned out, that in all SL's for fixed spacer thickness  $n$  the strength of IEC is almost independent on the magnetic layer thickness  $m$ . This seems to prove that in the SL's considered here, which are composed of two semiconductors with very different energy gaps, the valence electron mediated IEC is essentially an interface effect.

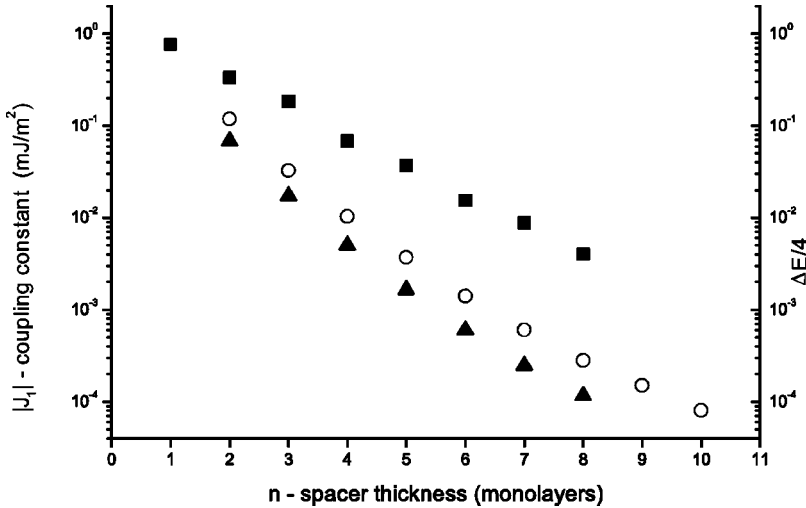


FIG. 6. The interlayer exchange constant  $J_1$  (left Y axis) as a function of the spacer thickness for ferromagnetic EuS/PbS (001) (squares) and (111) (triangles) SL's. For the antiferromagnetic EuTe/PbTe SL's (circles) the absolute value of the energy difference  $\Delta E$  was divided by four (at the right Y axis) for comparison with the FM case.

The dependence of the strength of the interlayer coupling on the spacer thickness  $n$  for all three studied types of SL's is presented in Fig. 6. We recall that for the [111] growth direction, we calculated IEC only for  $(n+m)/3 = \text{integer}$ , so that for these SL's in the figure, the points for different  $n$  values do not correspond to the same  $m$ . As can be seen in Fig. 6, the strength of the coupling in all three cases decreases with the spacer thickness approximately exponentially. The strongest and the least rapidly decreasing IEC was obtained in the case of the FM EuS/PbS (001) SL's. The comparison of the results obtained with the same set of model parameters for the two different types of EuS/PbS SL's (i.e., the SL's grown along [001] and [111] axis) indicates that the valence electron mediated IEC depends strongly on the lattice geometry. For example, for the PbS spacer  $n=2$  the obtained coupling between EuS (111) magnetic layers is about five times weaker than that between EuS (001) layers. Moreover, in the (111) SL's, the strength of the coupling decreases more quickly with  $n$ . The small regular deviations from the smooth dependence of  $J_1$  vs  $n$ , which can be best seen for every second  $n$  in the (001) case, but also for every third  $n$  in the (111) results, reflect the periodic effects of stacking.

Finally, we note that the IEC calculated for the AFM EuTe/PbTe (111) SL is stronger than that for FM EuS/PbS (111) SL (see Fig. 6). The difference in the band parameters by itself does not explain this result—the calculations performed for AFM and FM (111) SL's with identical sets of band parameters have shown that the coupling between the AFM layers is approximately two times stronger. This indicates that the interface region, important for the valence electron mediated IEC, is not limited to one layer of magnetic ions, but extends over two such monolayers.

#### IV. COMPARISON WITH THE EXPERIMENTAL DATA

##### A. Ferromagnetic EuS/PbS superlattices

The IEC was observed in ferromagnetic EuS/PbS (001) SL's by magnetic<sup>7</sup> and neutron diffraction and reflectivity<sup>6</sup> methods. For the samples with the thin enough spacers, i.e., 4.5 Å (1.5 monolayers, probably a mixture of  $n=2$  and  $n$

$=1$ ) and 10 Å ( $\sim n=3$ ), the antiferromagnetic interlayer coupling was observed in the magnetic moment measurements; the magnetic methods did not reveal any IEC in the samples with larger spacer thicknesses. In the neutronographic experiments, the AFM IEC was confirmed in the above two samples, but it was also observed in the sample with 23 Å PbS layers. Further measurements in the external magnetic fields, parallel to the layers, allowed us to estimate the experimental strength of the coupling constant  $J_1$ , from the magnetic field  $B$  erasing the AFM neutron reflectivity peak.<sup>25</sup> This was possible for the two samples with the thinner spacers, but not for the sample with the thicker spacer. For the latter, the field-induced changes in the neutronographic spectra were irreversible, what suggests that in this case the IEC was weaker than the magnetic anisotropies. The estimated experimental values of  $J_1$  are: 0.063, 0.031, and 0.019 (in mJ/m<sup>2</sup>), for  $n=1, 2$ , and 3, respectively.<sup>25</sup> The corresponding theoretical values obtained from our model are: 0.77, 0.33, and 0.18 mJ/m<sup>2</sup>. Thus, one can conclude, that the model of valence electron mediated IEC describes properly the sign and the rate of the decrease of the coupling with the spacer thickness, but overestimates the strength of the coupling. The fact that the theoretical results obtained for crystallographically perfect SL's lead to exchange constants order of magnitude larger than those observed for the real multilayer structures, is probably due to the interface diffusion, which in the case of metallic structures, was shown to reduce significantly the strength of the IEC.<sup>2</sup>

##### B. Antiferromagnetic EuTe/PbTe superlattices

Unfortunately, for the AFM type of SL's there are no experiments, which provide direct information about the strength of the coupling. The evidences of the existence of the coupling between the AFM EuTe layers come from the satellite structure of the neutron diffraction spectra, seen in a variety of EuTe/PbTe SL's consisting of several hundreds of periods.<sup>5,26</sup> The detailed analysis of the shapes of the satellite lines in the neutronographic spectra indicates that in these SL's, the EuTe layers are not entirely coupled, but only par-

tially correlated; the thicker the PbTe spacer layers, the weaker the correlation.<sup>26</sup> Under the strong assumption that the structures are morphologically perfect, with the same  $m$  and  $n$  values throughout the entire SL, this degree of correlation can be quantitatively determined. Under the same assumption, the analysis of the satellites positions allows us to distinguish which spin configuration, the in phase or out of phase, is dominating.

The observed spectra for the SL's with nominally even  $m$  and even  $n$  reveal the preference for the in-phase spin configurations, whereas those for the SL's with odd  $m$  and even  $n$  exhibit the preference for the out-of-phase configuration, both in agreement with the predictions of the present model. For the case of even  $m$  and odd  $n$  there are no available data. Finally, for the samples with  $m$  and  $n$  both odd, the neutron diffraction spectra suggest that the in-phase configuration is preferred, contrary to the theoretical predictions. However, the in-phase spin configuration for SL's with odd number of spin planes in each antiferromagnetic layer should exhibit ferrimagnetic properties, i.e., lead to a significant net magnetic moment of ferrimagnetic domains. No such magnetic moments were detected in these samples.<sup>27</sup> These somewhat confusing results seem to indicate that both chemical and magnetic structures of the studied SL's are not perfect enough. New technological and experimental efforts to observe the IEC in EuTe/PbTe SL's with smaller number of SL periods, i.e., in SL's with better controlled  $m$  and  $n$  values, are undertaken.

In conclusion, we have shown, within a 3D tight-binding model, that the valence electron mediated interlayer exchange coupling explains the AFM coupling between the FM layers observed in EuS/PbS (001) SL's with narrow PbS spacers. The strength of the calculated coupling depends strongly on the lattice geometry and decreases approximately exponentially with the spacer thickness  $n$ . For a given type of SL, it is almost independent on the number  $m$  of the spin planes within each magnetic layer. These features distinguish the considered mechanism from another mechanism of AFM coupling between the FM layers, namely, the dipolar coupling possible in multilayer structures with tiny magnetic domains.<sup>28</sup>

The valence electron mediated interlayer coupling is, up to now, the only effective mechanism capable to explain the origin of the interlayer correlations observed in the antiferromagnetic EuTe/PbTe SL's with no localized impurity states. The current, not complete understanding of the experimental data for AFM SL's, does not allow us, however, to draw definite conclusions about the comparison between the details of the experimental and theoretical results.

#### ACKNOWLEDGMENTS

This work was partially supported by the Polish Scientific Committee KBN, Grant No. 2 P03B 007 16.

- 
- <sup>1</sup>P. Grünberg, R. Schreiber, Y. Pang, M.B. Brodsky, and H. Sower, *Phys. Rev. Lett.* **57**, 2442 (1986).
- <sup>2</sup>P. Bruno, *Phys. Rev. B* **52**, 411 (1995); cond-mat/9905022, and references cited therein.
- <sup>3</sup>V. Nunez, T.M. Giebultowicz, W. Faschinger, G. Bauer, H. Sitter, and J.K. Furdyna, *J. Magn. Magn. Mater.* **140–144**, 633 (1995).
- <sup>4</sup>J.J. Rhyne, J. Lin, J.K. Furdyna, and T.M. Giebultowicz, *J. Magn. Magn. Mater.* **177–181**, 1195 (1998).
- <sup>5</sup>T.M. Giebultowicz, V. Nunez, G. Springholz, G. Bauer, J. Chen, M.S. Dresselhaus, and J.K. Furdyna, *J. Magn. Magn. Mater.* **140–144**, 635 (1995).
- <sup>6</sup>H. Kępa, J. Kutner-Pielaszek, A. Twardowski, A. Yu. Sipatov, C. F. Majkrzak, T. Story, R. R. Gałazka, T. M. Giebultowicz, *Proc. ICM, Recife, Brasil 2000*, *J. Magn. Magn. Mater.* (to be published).
- <sup>7</sup>K. Ha, C. H. W. Swüste, H. J. M. Swagten, A. A. Smits, W. J. M. de Jonge, T. Story, W. Dobrowolski, M. Arciszewska, R. R. Gałazka, A. Yu. Sipatov, *International Colloquium on Magnetic Thin Films and Surfaces, Natal, Brazil 2000*, Extended Abstracts.
- <sup>8</sup>N. Akiba, F. Matsukura, A. Shen, Y. Ohno, H. Ohno, A. Oiwa, S. Katsumoto, and Y. Iye, *Appl. Phys. Lett.* **73**, 2122 (1998); D. Chiba, N. Akiba, Y. Ohno, and H. Ohno, *ibid.* **77**, 1873 (2000).
- <sup>9</sup>P. Shevchenko, L. Świerkowski, and J. Oitmaa, *J. Magn. Magn. Mater.* **177–181**, 1168 (1998).
- <sup>10</sup>T.M. Rusin, *Phys. Rev. B* **58**, 2107 (1998).
- <sup>11</sup>H. Heinrich, *Lectures Notes in Physics* (Springer-Verlag, Heidelberg, 1980) Vol. 133, p. 407.
- <sup>12</sup>J. Blinowski and P. Kacman, *Acta Phys. Pol. A* **92**, 719 (1997).
- <sup>13</sup>M. Wilczyński and R. Świrkowicz, *Phys. Status Solidi B* **212**, 165 (1999).
- <sup>14</sup>V.K. Dugaev, V.I. Litvinov, W. Dobrowolski, and T. Story, *Solid State Commun.* **110**, 351 (1999).
- <sup>15</sup>Su-Huai Wei and A. Zunger, *Phys. Rev. B* **55**, 13 605 (1997).
- <sup>16</sup>P.J. Lin and L. Kleinman, *Phys. Rev.* **142**, 428 (1966).
- <sup>17</sup>P. Wachter, *Handbook on the Physics and Chemistry of Rare Earths*, edited by K. A. Gschneidner and L. Eyring (North-Holland, Amsterdam, 1979), p. 507.
- <sup>18</sup>S.J. Cho, *Phys. Rev. B* **1**, 4589 (1970).
- <sup>19</sup>G. Guentherodt, *Phys. Kondens. Mater.* **18**, 37 (1974).
- <sup>20</sup>S. Mathi Jaya and W. Nolting, *J. Phys.: Condens. Matter* **9**, 10 439 (1997).
- <sup>21</sup>A. Stachow-Wojcik, T. Story, W. Dobrowolski, M. Arciszewska, R.R. Gałazka, M.W. Kreijveld, C.H.W. Swüste, H.J.M. Swagten, W.J.M. de Jonge, A. Twardowski, and A.Yu. Sipatov, *Phys. Rev. B* **60**, 15 220 (1999).
- <sup>22</sup>I.N. Goncharenko and I. Mirebeau, *Phys. Rev. Lett.* **80**, 1082 (1998).
- <sup>23</sup>W. A. Harrison, *Electronic Structure and the Properties of Solids* (Freeman, San Francisco, 1980).
- <sup>24</sup>S.S.P. Parkin, *Phys. Rev. Lett.* **67**, 3598 (1991).
- <sup>25</sup>H. Kępa, J. Kutner-Pielaszek, J. Blinowski, A. Twardowski, C.F. Majkrzak, T. Story, P. Kacman, R.R. Gałazka, K. Ha, H.J.M.

- Swagten, W.J.M. de Jonge, A.Yu. Sipatov, T.M. Giebultowicz, cond-mat/0102194 (unpublished).
- <sup>26</sup>H. Kępa, J. Blinowski, P. Kacman, G. Springholz, G. Bauer, C. F. Majkrzak, K. I. Goldman, and T. M. Giebultowicz, in *Proceedings of the 24th International Conference on the Physics of Semiconductors*, edited by D. Gershoni (World Scientific, Singapore 1999).
- <sup>27</sup>S. Holl, F. Schinagl, T.M. Giebultowicz, and H. Krenn, *J. Magn. Mater.* **220**, 293 (2000).
- <sup>28</sup>J.A. Borchers, P.M. Gehring, R.W. Erwin, J.F. Ankner, C.F. Majkrzak, T.L. Hylton, K.R. Coffey, M.A. Parker, and J.K. Howard, *Phys. Rev. B* **54**, 9870 (1996).